

Convergence rates of recursive Newton-type methods for multifrequency scattering problems

Mourad Sini^a and Nguyen Trung Thành^b

^aJohann Radon Institute for Computational and Applied Mathematics (RICAM), Austrian Academy of Sciences, Linz, Austria. Email: mourad.sini@oeaw.ac.at

^bDepartment of Mathematics & Statistics, University of North Carolina at Charlotte, Charlotte 28223, NC, USA. Email: tnguy152@uncc.edu.

Abstract

We are concerned with the reconstruction of a sound-soft obstacle using far field measurements of the scattered waves associated with incident plane waves sent from one direction but at multiple frequencies. We define, for each frequency, the observable shape as the one which is described by finitely many modes and produces a far field pattern close to the measured one. In the first step, we propose a recursive Newton-type method for the reconstruction of the observable shape at the highest frequency knowing an estimate of the observable shape at the lowest frequency. We analyze its convergence and derive its convergence rate in terms of the frequency step, the number of the Newton iterations and the noise level. In the second step, we design a multilevel Newton method which has the same convergence rate as the one described in the first step but avoids the need of a good estimate of the observable shape at the lowest frequency and a small frequency step (or a large number of Newton iterations). The performances of the proposed algorithms are illustrated with numerical results using simulated data.

Keywords: Inverse obstacle scattering, multifrequency, convergence, Newton method.

AMS classification codes: 35R30, 65N21, 78A46.

1 Introduction

We consider the problem of reconstructing the shape of a two-dimensional sound-soft acoustic obstacle using far field measurements associated with incident plane waves sent from only one incident direction but at multiple frequencies. The forward scattering problem can be represented by the following two-dimensional Dirichlet boundary value problem

$$\Delta u(x) + k^2 u(x) = 0, \quad x \in \mathbb{R}^2 \setminus \bar{D}, \quad (1)$$

$$u(x) = 0, \quad x \in \partial D, \quad (2)$$

$$\lim_{|x| \rightarrow \infty} \sqrt{|x|} \left[\frac{\partial u^s(x)}{\partial |x|} - iku^s(x) \right] = 0, \quad (3)$$

where k is the wavenumber, u is the total wave and $u^s := u - u^i$ is the scattered wave. Here, u^i is the incident plane wave given by $u^i(x) := e^{ikx \cdot \theta}$ with $\theta \in \mathbb{S}^1 := \{x \in \mathbb{R}^2 : |x| = 1\}$ being the direction of incidence. The well-posedness of the problem (1)–(3) for each wavenumber k is well-known under the assumption that ∂D is Lipschitz (see, e.g., [20]). Moreover, we have the following asymptotic behavior of the scattered field u^s at infinity

$$u^s(x) = \frac{e^{ik|x|}}{\sqrt{|x|}} u^\infty(\hat{x}) + O(|x|^{-3/2}), \quad |x| \rightarrow \infty, \quad (4)$$

where $\hat{x} := x/|x|$ and u^∞ is an analytic function on \mathbb{S}^1 referred to as the *far field pattern* of the scattered field u^s .

The inverse problem we investigate here is *to reconstruct the obstacle D from measured far field patterns $u^\infty(\hat{x}, k)$, $\hat{x} \in \mathbb{S}^1$, for **one** direction of incidence $\theta \in \mathbb{S}^1$ and multiple wavenumbers k in the interval $[k_l, k_h]$ ($0 < k_l < k_h$)*. Here we denote the far field pattern by $u^\infty(\hat{x}, k)$ to emphasize its dependence on the wavenumber k .

Let us recall some known results concerning this problem. It has a unique solution if a band of wavenumbers $[k_l, k_h]$ is used, see, e.g., [23]. If the measurements correspond to a finite number of frequencies, as we consider in this paper, then the uniqueness of the solution is guaranteed if the lowest frequency is small enough, see, e.g., [11, 14]. For local uniqueness at each frequency, we refer to [26]. If more *a priori* information about the obstacle's shape is available, then some global uniqueness results at an arbitrary but fixed frequency have been published. For example, if the obstacles are polygonal, see [1, 8] and if these obstacles are nowhere analytic, see [17]. Regarding the stability issue, *loglog* stability estimates are given in [18] and an improved *log* stability estimate is shown in [24]. In the high frequency regime, a conditional asymptotic Hölder stability estimate in the part of the boundary ∂D , of a convex obstacle D , illuminated by the incident plane wave u^i is obtained in [25].

The main advantage of using multifrequency data is that it can help to obtain accurate reconstructions without the need for a good initial guess. Let us explain the reasons why we can expect these two features. The first one is that since the size of the domain in which the inverse problem is uniquely solvable is inversely proportional to the used frequency, the one in which the objective functional has a unique minimum is also inversely proportional to that frequency, as proved in [25]. Due to this fact, if the lowest frequency used is small enough, it is not necessary to start from a good initial guess in solving for its unique minimum. The second one is related to the fact that, as discussed in [5], for each frequency the dimension of the retrievable information is small which is due to the instability of the original problem. Therefore, at each frequency, we only need to choose a relatively small number of unknown parameters in the shape representation, which reduces the instability issue of the reconstruction problem. The third one is that at high frequencies the problem becomes more stable, i.e. more details of the obstacle can be reconstructed. However, there are more local minima of the objective functional. Using the reconstruction result at a lower frequency helps to avoid getting a false local minimum.

Different reconstruction methods using multifrequency data have been proposed in

the last two decades or so. The first type of method is known as frequency-hopping algorithms which use the reconstruction at a frequency as an initial guess at a higher frequency with the hope that this initial guess falls within the convergence domain of the objective functional. Several numerical results, using either simulated data, see e.g. [3, 9, 7, 25], or experimental data, see, e.g. [4, 27, 28], have been demonstrated. However, convergence of this type of algorithms was only investigated in [3, 25] for the so-called recursive linearization algorithm (RLA) proposed in [7]. Another type of methods using multifrequency/multiwaves data, related to the sampling methods, can be found in [15, 16, 22].

Inspired by the presentation in [7], we define, for each frequency, the observable shape as the one which is described by finitely many modes and produces a far field pattern close to the measured one. Our goal then is to reconstruct the observable shape at the highest available frequency κ_h . The link between this observable shape and the true one is related to the stability issue, see [25] and section 2.3 for more explanation. To achieve this goal, we proceed as follows.

- First, we propose a projected recursive Newton method for solving this inverse problem. The idea is to use a certain number of Newton iterations at each frequency, starting from the lowest one, and then the reconstruction is used to linearize the problem at the next higher frequency. We prove the convergence rate of this algorithm, see section 2, which shows a significant improvement compared to the linear convergence rate of the RLA obtained in [3, 25]. We investigate both noiseless and noisy data.
- Second, a multi-level Newton method is proposed and its convergence rate is also investigated. The main idea of this method is to divide the whole frequency set into subsets and each of them are treated using the recursive Newton algorithm of section 2. The difference between these two methods is that in multi-level Newton method the regularization parameter associated with different frequency subsets can be chosen to be different whereas in the original recursive Newton method this parameter is fixed at all frequencies. This adaptive choice of the regularization parameter allows us to obtain the same convergence rate as the previous algorithm but with less restrictive requirement on the accuracy of the reconstruction at the lowest frequency. This topic is discussed in section 3. Related to this approach, we cite the work [12] which also investigates a multi-level projected steepest descent method in Banach spaces with a discrepancy principle used for stopping the iterative process at each frequency.

Finally, we show in section 4 some numerical results using simulated data to demonstrate the performance of the aforementioned algorithms. Our numerical results are consistent with the theoretical analysis of sections 2 and 3.

Concerning the choice of the first guess at the starting frequency as well as the reconstruction accuracy, we refer the reader to section 3 of [25].

2 A projected recursive Newton method and its convergence rate

In this work, we consider the case of star-shaped obstacles whose boundary ∂D can be represented by

$$\partial D = \{x(t) \in \mathbb{R}^2 : x(t) = x^0 + r(t)(\cos t, \sin t), t \in [0, 2\pi]\}, \quad (5)$$

where x^0 is a given internal point of D in \mathbb{R}^2 and the radial function r is positive in $[0, 2\pi]$ with $r(0) = r(2\pi)$. In the following, we denote by $D(r)$ to indicate the dependence of the obstacle on its radial function r . For each wavenumber k , we define the *boundary-to-far field operator* (or *far field operator*, in short) $F(\cdot, k)$ which maps each radial function r to the far field pattern $u^\infty(\cdot, k, r)$ of the forward scattering problem (1)–(3) with $D = D(r)$. In this paper, we assume that the shape is of class C^3 , i.e., the 2π -periodic extension of the radial function r from $[0, 2\pi]$ to \mathbb{R} belongs to $C^3(\mathbb{R})$. This smoothness guarantees the regularity of the derivatives of the far field operator used in section 2.2. We denote by X_{ad} the set of radial functions of this C^3 -class starlike shapes. This set is considered as the admissible set in our algorithm.

Let X be a Hilbert space which contains the admissible set X_{ad} . In this work, we choose this space to be $X := L_2[0, 2\pi]$. However other spaces can be used as well. Therefore, for generality, in the following we use the notation X instead of L_2 . The derivative of F with respect to the radial function, $\partial_r F(r, k)$, is defined by

$$\partial_r F(r, k)a := \lim_{\epsilon \rightarrow 0} \frac{F(r + \epsilon a, k) - F(r, k)}{\epsilon},$$

for $a \in X$. Note that $\partial_r F(r, k)$ is an injective linear operator from X to $L_2(\mathbb{S}^1)$ for $r \in X_{ad}$, see [19, 10]. We also refer to these references for its characterization.

In the following sections, we denote by $u_m^{\infty, \delta}(\cdot, k) \in L_2(\mathbb{S}^1)$ the noisy measured far field pattern at the wavenumber k with additive random noise of magnitude (noise level) $\delta \geq 0$. We define the operator \tilde{F}_δ from X_{ad} to $L_2(\mathbb{S}^1)$ by $\tilde{F}_\delta(r, k) := F(r, k) - u_m^{\infty, \delta}(\cdot, k)$. The norms in X and $L_2(\mathbb{S}^1)$ are denoted by $\|\cdot\|_X$ and $\|\cdot\|_2$, respectively.

2.1 Description of the algorithm

Suppose that the far field pattern is measured at the discrete set of frequencies $k_n := k_l + n\Delta k$, $n = 0, 1, \dots, N$, with $\Delta k = \frac{k_h - k_l}{N}$. Consider a set of increasing subspaces $X_0 \subset X_1 \subset \dots \subset X_N$ of X . The choice of these subspaces will be discussed later in section 2.2. We denote by P_n the orthogonal projection of X onto X_n , $n = 0, 1, \dots, N$. Assume further that we have a rough approximation $r_0 \in X_0$ of the exact radial function at the lowest frequency $k_0 = k_l$, which can be obtained by minimizing the least-squares objective functional as described in the first step of [25]. Given an integer $J > 0$ and an approximation $r_n \in X_n$ of the radial function at wavenumber k_n , we denote by $r_{n+1}^0 := r_n$ and consider J Newton

iterations at wavenumber k_{n+1} as follows: $r_{n+1}^{j+1} := r_{n+1}^j + P_{n+1}\Delta r_{n+1}^j$, $j = 0, \dots, J-1$, with Δr_{n+1}^j being the solution of the regularized least-squares minimization problem

$$\Delta r_{n+1}^j := \operatorname{argmin}_{\Delta r} \left\{ \frac{1}{2} \|\tilde{F}_\delta(r_{n+1}^j, k_{n+1}) + \partial_r F(r_{n+1}^j, k_{n+1})\Delta r\|_2^2 + \frac{1}{2}\alpha \|\Delta r\|_X^2 \right\} \quad (6)$$

with $\alpha > 0$. The solution to (6) is given by

$$\Delta r_{n+1}^j = -[\alpha I + (A_{n+1}^j)^* A_{n+1}^j]^{-1} (A_{n+1}^j)^* \tilde{F}_\delta(r_{n+1}^j, k_{n+1}),$$

where $A_{n+1}^j := \partial_r F(r_{n+1}^j, k_{n+1})$ and $(A_{n+1}^j)^*$ is its adjoint operator. Hence,

$$r_{n+1}^{j+1} := r_{n+1}^j - P_{n+1}[\alpha I + (A_{n+1}^j)^* A_{n+1}^j]^{-1} (A_{n+1}^j)^* \tilde{F}_\delta(r_{n+1}^j, k_{n+1}), j = 0, \dots, J-1, \quad (7)$$

Since $r_{n+1}^0 = r_n \in X_n \subset X_{n+1}$, the approximations r_{n+1}^j also belong to the subspace X_{n+1} for $j = 1, \dots, J$. We choose $r_{n+1} := r_{n+1}^J \in X_{n+1}$ as the reconstruction at the wavenumber k_{n+1} . This process is repeated until the highest wavenumber $k_N = k_h$. The algorithm is summarized as follows.

Algorithm 2.1.

- Given measured data $u_m^{\infty, \delta}(\cdot, k)$ for $k = k_0, \dots, k_N$, the parameter $\alpha > 0$ and the subspaces X_n , $n = 0, \dots, N$.
- Step 1: find an approximation $r_0 \in X_0$ at frequency k_0 .
- Step 2 (recurrence) For $n = 0, \dots, N-1$
 - Set $r_{n+1}^0 := r_n$.
 - For $j = 0, \dots, J-1$
 - * Compute $\tilde{F}_\delta(r_{n+1}^j, k_{n+1})$, A_{n+1}^j and $(A_{n+1}^j)^*$.
 - * Compute $r_{n+1}^{j+1} := r_{n+1}^j - P_{n+1}[\alpha I + (A_{n+1}^j)^* A_{n+1}^j]^{-1} (A_{n+1}^j)^* \tilde{F}_\delta(r_{n+1}^j, k_{n+1})$.
 - End (for j)
 - Set $r_{n+1} := r_{n+1}^J$.
- End (for n).

Remark 2.1.

1. In the recursive linearization algorithm, as discussed in [3, 7, 25], only one Newton step is used at each frequency. In other words, the reconstruction at k_{n+1} is chosen by $r_{n+1} := r_{n+1}^1$.

2. The stopping criteria in Algorithm 2.1 is related to a trade-off between the frequency step Δk (or the number of N of the used frequencies) and the number J of the Newton iterations to achieve a final error of the order $O(\delta^{\frac{2}{3}})$, see Remark 2.2.

To implement Algorithm 2.1, it is necessary to represent the radial function r as a function of a finite number of parameters. Since any radial function $r(t)$ satisfies $r(0) = r(2\pi)$, it can be considered as a periodic function with the period of 2π . Hence, we can represent it as the following Fourier series

$$r(t) = \beta_0 + \sum_{m=1}^{\infty} (\beta_m \cos mt + \gamma_m \sin mt). \quad (8)$$

We note that the Fourier coefficients β_m and γ_m converge to zero as $m \rightarrow \infty$. Their convergence rate depends on the smoothness of the function $r(t)$, see [13]. For each number $M \in \mathbb{N}$, we define the cut-off approximation $r^M(t)$ of $r(t)$ by

$$r^M(t) := \beta_0 + \sum_{m=1}^M (\beta_m \cos mt + \gamma_m \sin mt). \quad (9)$$

It is clear that, for large M , r^M is different from r just in high frequency modes which represent small details of the obstacle shape. Let us recall the notion of *finite dimensional observable shapes* which was defined in [25]. For a given value $\tilde{\delta} > \delta$, there exists a number $M_0(k) \in \mathbb{N}$ depending on k such that $\|F(r^M, k) - F(r, k)\|_2 \leq \tilde{\delta} - \delta$ for all $M \geq M_0(k)$. Consequently, $\|F(r^M, k) - u_m^{\infty, \delta}(\cdot, k)\|_2 \leq \tilde{\delta}$ for $M \geq M_0(k)$. Note that $M_0(k)$ also depends on $\tilde{\delta}$ and δ , but we ignore these parameters since they are fixed throughout the paper. From this analysis, we can simplify the inverse problem by determining the cut-off approximation r^M (or its Fourier coefficients) instead of the radial function r itself. By this simplification, the inverse problem becomes finite dimensional.

In the following analysis, we choose the subspaces X_n of X containing all functions of the form (9) with $M := M_n$ depending on n , that means X_n is spanned by the basis $\{1, \cos t, \sin t, \dots, \cos M_n t, \sin M_n t\}$. We denote by $X_n^+ := \{\varphi \in X_n : \varphi(t) > 0, \forall t \in [0, 2\pi]\}$. Since functions in X_n are smooth, we have $X_n^+ \subset X_{ad}$.

Definition 2.2. For each wavenumber k and a given $\tilde{\delta} > \delta$, a *finite dimensional observable shape* (or, in short, *observable shape*) $D(\tilde{r}(k))$ is defined as a domain of which the radial function $\tilde{r}(k) \in X_M^+$ for some $M \in \mathbb{N}$ and the corresponding far field pattern $F(\tilde{r}(k), k)$ satisfies the condition $\|F(\tilde{r}(k), k) - u_m^{\infty, \delta}(\cdot, k)\|_2 \leq \tilde{\delta}$.

By this definition, a finite dimensional observable shape basically produces the same measured data as the true one (up to the noise level) but usually has a simpler Fourier series. It is obvious that $D(r^M)$ is a finite dimensional observable shape of the obstacle $D(r)$ for $M \geq M_0(k)$. However, we should emphasize that, there may be several finite dimensional observable shapes which are very different from $D(r^M)$ due to the ill-posedness of the considered inverse problem. The question on how these observable shapes approximate the original one relates closely to the stability of the inverse problem which was discussed in [25].

As remarked in [25], we made use of the value $\tilde{\delta}$ instead of the noise level δ because if the latter is used, the finite dimensional observable shapes might not exist. However, it is

possible to choose $\tilde{\delta}$ close to δ while $M_0(k)$ can still be chosen not too large. This can be explained using the Heisenberg's uncertainty principle in Physics on the resolution limit of scattering problems. It says that, at a fix frequency, we cannot observe small details of the scatterer using noisy measurements of the far field pattern, regardless the noise magnitude. In other words, choosing too many Fourier modes does not help to improve the reconstruction accuracy but increases the instability of the reconstruction. Therefore, $M_0(k)$ should not be chosen too large. As shown in [7], this resolution limit is about half of the wavelength for weak penetrable scatterers, see also [2, 3]. Due to this uncertainty principle, we also choose r_n , $n = 0, \dots, N$, in Algorithm 2.1 such that they contain finite numbers of Fourier modes.

2.2 Convergence rate

Algorithm 2.1 requires an approximation r_0 of the true radial function at the lowest frequency. As proved in [25], we can only guarantee a “good” r_0 if the true obstacle D is contained in the disk $B(x^0, \frac{\pi}{k_l})$ centered at the point x^0 and radius $\frac{\pi}{k_l}$. Therefore, we first assume that the unknown obstacle is within a given region and the lowest frequency k_l is chosen so small that this region is contained inside the disk $B(x^0, \frac{\pi}{k_l})$. Moreover, in the sequel, we make the following assumptions about the radial functions of the observable shapes:

Assumption 1: The radial functions $\tilde{r}(k_n)$, $n = 0, \dots, N$, are bounded from below, i.e., there exists a constant $\tilde{c} > 0$ such that

$$\tilde{c} \leq \|\tilde{r}(k_n)\|, \text{ for all } n, \quad (10)$$

where $\|\cdot\|$ represents the maximum norm. Since the observable shapes, roughly speaking, are approximations of the true one, the assumption (10) requires that the size of the true obstacle is not too small. As indicated in Theorem 2.4, this lower bound \tilde{c} can be chosen comparable to the regularization parameter α , see (21), which is reasonably small. That means, this assumption is not very restrictive.

Assumption 2: There exists a constant $d_0 \geq 1$ such that

$$\|\tilde{r}(k_{n+1}) - \tilde{r}(k_n)\|_X \leq d_0 |k_{n+1} - k_n|, \forall n = 0, \dots, N - 1. \quad (11)$$

Roughly speaking, this assumption says that the observable shapes of two consecutive frequencies should not be too different. For more details about the validity of Assumption 2, see Remark 3 of [25].

For the following convergence analysis, we assume that the subspaces X_n , $n = 0, \dots, N$ are chosen such that they contain the radial functions $\tilde{r}(k_n)$ of the observable shapes. We denote by $\tilde{A}_n := \partial_r F(\tilde{r}(k_n), k_n)$, $n = 0, 1, \dots, N$ and σ_n the smallest singular value of \tilde{A}_n restricted to X_{n+1} , $\tilde{A}_n|_{X_{n+1}}$, for $n = 0, \dots, N - 1$. Since these operators are injective, we have $\sigma_n > 0$, $n = 0, \dots, N - 1$. Finally we define

$$\sigma := \min\{\sigma_0, \dots, \sigma_{N-1}\}. \quad (12)$$

For the radial functions $\tilde{r}(k), k \in [k_l, k_h]$ associated with a given set of observable shapes of r , we write the operator \tilde{F}_δ as

$$\tilde{F}_\delta(r, k) = \tilde{F}(r, k) + f^{\tilde{\delta}}(\tilde{r}(k), k) \quad (13)$$

with $\tilde{F}(r, k) := F(r, k) - F(\tilde{r}(k), k)$ and $f^{\tilde{\delta}}(\tilde{r}(k), k) := F(\tilde{r}(k), k) - u_m^{\infty, \tilde{\delta}}(\cdot, k)$. Note that $\|f^{\tilde{\delta}}(\tilde{r}(k), k)\|_2 \leq \tilde{\delta}$. It is obvious that

$$\tilde{F}(\tilde{r}(k), k) = 0, \forall k \in [k_l, k_h]. \quad (14)$$

Note that $F(r, k)$ is twice continuously differentiable (see Remark 1 of [25]). Therefore, there exist some positive constants $d_i, i = 1, \dots, 4$, such that for all $r \in B(\frac{\pi}{k_l})$ and $k \in [k_l, k_h]$, we have

$$\begin{aligned} \|\partial_r \tilde{F}(r, k)\|_{\mathcal{L}(X, Y)} &\leq d_1, \quad \|\partial_k \tilde{F}(r, k)\|_2 \leq d_2, \\ \|\partial_{rr}^2 \tilde{F}(r, k)\|_{\mathcal{L}(X \times X, Y)} &\leq d_3, \quad \|\partial_{kr}^2 \tilde{F}(r, k)\|_{\mathcal{L}(X, Y)} \leq d_4. \end{aligned} \quad (15)$$

In this section, we need the following estimates concerning compact linear operators.

Lemma 2.3. *Let A be a compact linear operator from a Hilbert space X to a Hilbert space Y and $R_\alpha(A) := (\alpha I + A^*A)^{-1}A^*$ with $\alpha > 0$. Then*

$$\|(\alpha I + A^*A)^{-1}\|_{\mathcal{L}(X, X)} \leq \frac{1}{\alpha}, \quad (16)$$

$$\|R_\alpha(A)\|_{\mathcal{L}(Y, X)} \leq \frac{1}{2\sqrt{\alpha}}, \quad (17)$$

$$\|R_\alpha(A)A\|_{\mathcal{L}(X, X)} \leq 1. \quad (18)$$

Moreover, if \tilde{A} is also a compact linear operator from X to Y , we have

$$\|R_\alpha(A) - R_\alpha(\tilde{A})\|_{\mathcal{L}(Y, X)} \leq \frac{9}{4\alpha} \|A - \tilde{A}\|_{\mathcal{L}(X, Y)}. \quad (19)$$

We first prove the following result for the case of noiseless data.

Theorem 2.4. *Assume that the radial functions $\tilde{r}(k_n), n = 0, \dots, N$, of the observable shapes satisfy Assumptions 1 and 2. Let $X_n, n = 0, \dots, N$, be the subspaces of X containing these radial functions. Let $r_n, n = 0, \dots, N$, be given by Algorithm 2.1 with \tilde{F}_δ being replaced by \tilde{F} . Then for a fixed positive real number ϵ , $0 < \epsilon < 3/(2 + d_0)$, and for the regularization parameter α satisfying*

$$\alpha \leq \frac{\epsilon \sigma^2}{3 - \epsilon}, \quad (20)$$

there exists an integer N_0 depending on ϵ and α such that if

$$\|\tilde{r}(k_l) - r_0\|_X \leq d_0 c_0 \alpha < \tilde{c}, \quad (21)$$

with

$$c_0 := \frac{4\epsilon}{3d_3(9d_1 + \sqrt{\alpha})}, \quad (22)$$

then we have $r_n(t) > 0 \forall t \in [0, 2\pi]$ and the following error estimate holds true

$$\|\tilde{r}(k_n) - r_N\|_X \leq C_1 \left(\frac{\epsilon(1+d_0)}{3} \right)^{J-1} \sqrt{\Delta k}, \forall N \geq N_0, \quad (23)$$

where C_1 is a constant independent of α and N .

Proof. For $n = 0, \dots, N$ and $j = 0, \dots, J$, we denote by $e_n := \tilde{r}(k_n) - r_n$, $R_n^j := [\alpha I + (A_n^j)^* A_n^j]^{-1} (A_n^j)^*$ and $\tilde{R}_n := (\alpha I + \tilde{A}_n^* \tilde{A}_n)^{-1} \tilde{A}_n^*$. We also denote by $e_{n+1}^j := \tilde{r}(k_{n+1}) - r_{n+1}^j$ for $j = 1, \dots, J; n = 1, \dots, N$.

We first estimate e_{n+1}^1 . Here we repeat some arguments of [3, 25]. It follows from (7) that

$$\begin{aligned} e_{n+1}^1 &= \tilde{r}(k_{n+1}) - r_{n+1}^0 + P_{n+1} R_{n+1}^0 \tilde{F}(r_{n+1}^0, k_{n+1}) \\ &= \tilde{r}(k_{n+1}) - \tilde{r}(k_n) + \tilde{r}(k_n) - r_{n+1}^0 - P_{n+1} \tilde{R}_n \tilde{A}_n e_n \\ &\quad + P_{n+1} \left[\tilde{R}_n \tilde{A}_n e_n + R_{n+1}^0 \tilde{F}(r_{n+1}^0, k_{n+1}) \right]. \end{aligned} \quad (24)$$

We recall that $r_{n+1}^0 = r_n$. Let us evaluate the right hand side. Firstly, the first two terms are bounded by (11). Secondly, note that since $\tilde{r}(k_n), r_n \in X_n \subset X_{n+1}$, we have $\tilde{r}(k_n) - r_{n+1}^0 = P_{n+1} e_n$. The spectral theory implies that

$$\|P_{n+1} [e_n - \tilde{R}_n \tilde{A}_n e_n]\|_X \leq \frac{\alpha}{\alpha + \sigma^2} \|e_n\|_X. \quad (25)$$

Thirdly,

$$\begin{aligned} \tilde{R}_n \tilde{A}_n e_n + R_{n+1}^0 \tilde{F}(r_{n+1}^0, k_{n+1}) &= \tilde{R}_n [\tilde{A}_n e_n + \tilde{F}(r_n, k_n)] - (\tilde{R}_n - R_{n+1}^0) \tilde{F}(r_n, k_n) \\ &\quad + R_{n+1}^0 [\tilde{F}(r_n, k_{n+1}) - \tilde{F}(r_n, k_n)]. \end{aligned} \quad (26)$$

Using the Taylor expansion of $\tilde{F}(r_n, k_n)$ at $\tilde{r}(k_n)$ up to the second order, (17) and (14)–(15), we have

$$\|\tilde{R}_n [\tilde{A}_n e_n + \tilde{F}(r_n, k_n)]\|_X \leq \frac{d_3}{4\sqrt{\alpha}} \|e_n\|_X^2. \quad (27)$$

On the other hand, it follows from Lemma 2.3 and (14)–(15) that

$$\begin{aligned} \|(\tilde{R}_n - R_{n+1}^0) \tilde{F}(r_n, k_n)\|_X &\leq \frac{9}{4\alpha} \|A_{n+1}^0 - \tilde{A}_n\|_{\mathcal{L}(X,Y)} \|\tilde{F}(r_n, k_n) - \tilde{F}(\tilde{r}(k_n), k_n)\|_2 \\ &\leq \frac{9d_1}{4\alpha} \|A_{n+1}^0 - \tilde{A}_n\|_{\mathcal{L}(X,Y)} \|e_n\|_X. \end{aligned}$$

From the definition of A_{n+1}^0 and \tilde{A}_n we have

$$\begin{aligned} \|A_{n+1}^0 - \tilde{A}_n\|_{\mathcal{L}(X,Y)} &\leq \|\partial_r \tilde{F}(r_n, k_{n+1}) - \partial_r \tilde{F}(r_n, k_n)\|_{\mathcal{L}(X,Y)} \\ &\quad + \|\partial_r \tilde{F}(r_n, k_n) - \partial_r \tilde{F}(\tilde{r}(k_n), k_n)\|_{\mathcal{L}(X,Y)} \\ &\leq \Delta k d_4 + d_3 \|e_n\|_X. \end{aligned}$$

Replacing this estimate into the above inequality we obtain

$$\|(\tilde{R}_n - R_{n+1}^0)\tilde{F}(r_n, k_n)\|_X \leq \frac{9d_1}{4\alpha} [\Delta k d_4 + d_3 \|e_n\|_X] \|e_n\|_X. \quad (28)$$

It follows from (15) that

$$\|R_{n+1}^0[\tilde{F}(r_n, k_{n+1}) - \tilde{F}(r_n, k_n)]\|_X \leq \frac{d_2}{2\sqrt{\alpha}} \Delta k. \quad (29)$$

Substituting (27)–(29) into (26), we obtain

$$\|P_{n+1} \left[\tilde{R}_n \tilde{A}_n e_n + R_{n+1}^0 \tilde{F}(r_n, k_{n+1}) \right]\|_X \leq \frac{d_2}{2\sqrt{\alpha}} \Delta k + \left(\frac{9d_1 d_3}{4\alpha} + \frac{d_3}{4\sqrt{\alpha}} \right) \|e_n\|_X^2. \quad (30)$$

By combining (11), (25) and (30) we have

$$\begin{aligned} \|e_{n+1}^1\|_X &\leq \Delta k \left(d_0 + \frac{d_2}{2\sqrt{\alpha}} \right) + \frac{\alpha}{\alpha + \sigma^2} \|e_n\|_X \\ &\quad + \frac{9d_1 d_4}{4\alpha} \Delta k \|e_n\|_X + \left(\frac{9d_1 d_3}{4\alpha} + \frac{d_3}{4\sqrt{\alpha}} \right) \|e_n\|_X^2. \end{aligned} \quad (31)$$

Let us estimate the right hand side of (31). First, it follows from (20) that

$$\frac{\alpha}{\alpha + \sigma^2} \leq \frac{\epsilon}{3}, \quad (32)$$

Next, if $\|e_n\|_X \leq d_0 c_0 \alpha$, from (22) we have

$$\left(\frac{9d_1 d_3}{4\alpha} + \frac{d_3}{4\sqrt{\alpha}} \right) \|e_n\|_X = \frac{\epsilon}{3c_0\alpha} \|e_n\|_X \leq \frac{d_0\epsilon}{3}. \quad (33)$$

For the chosen α , we can also choose a number $N_0 = N_0(\alpha)$ such that for all $N \geq N_0$, we have

$$\frac{9d_1 d_4}{4\alpha} \Delta k \leq \frac{\epsilon}{3} \quad (34)$$

and

$$\Delta k \left(1 + \frac{d_2}{2d_0\sqrt{\alpha}} \right) \leq \left[1 - \frac{\epsilon}{3}(2 + d_0) \right] c_0 \alpha. \quad (35)$$

Note that the right hand side is positive. It follows from (31)–(35) that

$$\|e_{n+1}^1\|_X \leq \left[1 - \frac{\epsilon}{3}(2 + d_0) \right] d_0 c_0 \alpha + \frac{\epsilon}{3}(2 + d_0) \|e_n\|_X \leq d_0 c_0 \alpha.$$

Next, we estimate e_{n+1}^{j+1} for $j = 1, \dots, J-1$. We rewrite them in the form

$$\begin{aligned} e_{n+1}^{j+1} &= \tilde{r}(k_{n+1}) - r_{n+1}^j + P_{n+1} R_{n+1}^j \tilde{F}(r_{n+1}^j, k_{n+1}) \\ &= P_{n+1} \left[e_{n+1}^j - \tilde{R}_{n+1}^j \tilde{A}_{n+1} e_{n+1}^j \right] + P_{n+1} \tilde{R}_{n+1}^j \tilde{A}_{n+1} e_{n+1}^j + P_{n+1} R_{n+1}^j \tilde{F}(r_{n+1}^j, k_{n+1}). \end{aligned} \quad (36)$$

By the same arguments as above, we obtain

$$\|e_{n+1}^{j+1}\|_X \leq \frac{\alpha}{\alpha + \sigma^2} \|e_{n+1}^j\|_X + \left(\frac{9d_1d_3}{4\alpha} + \frac{d_3}{4\sqrt{\alpha}} \right) \|e_{n+1}^j\|_X^2.$$

Hence, under the same conditions (32) and (33)

$$\|e_{n+1}^{j+1}\|_X \leq \frac{\epsilon}{3} (1 + d_0) \|e_{n+1}^j\|_X < \|e_{n+1}^j\|_X, j = 1, \dots, J-1. \quad (37)$$

Therefore, if $\|e_0\|_X \leq d_0 c_0 \alpha$, we can prove by recurrence that $\|e_n^j\|_X \leq d_0 c_0 \alpha$ for $j = 1, \dots, J$ and $n = 1, \dots, N$. From this it is clear that

$$r_n^j(t) \geq \tilde{r}(k_n, t) - e_n^j(t) \geq \tilde{c} - d_0 c_0 \alpha > 0 \text{ for all } j \text{ and } n.$$

Hence, $r_n(t) > 0$ for all n . Moreover,

$$\|e_{n+1}\|_X \leq \left(\frac{\epsilon(1+d_0)}{3} \right)^{J-1} \left[\Delta k \left(d_0 + \frac{d_2}{2\sqrt{\alpha}} \right) + \frac{\epsilon(2+d_0)}{3} \|e_n\|_X \right], \forall n = 0, \dots, N-1.$$

Consequently,

$$\begin{aligned} \|e_N\|_X &\leq \left(\frac{\epsilon(1+d_0)}{3} \right)^{J-1} \Delta k \left(d_0 + \frac{d_2}{2\sqrt{\alpha}} \right) \frac{1}{1 - \left(\frac{\epsilon(1+d_0)}{3} \right)^{J-1} \frac{\epsilon(2+d_0)}{3}} \\ &\quad + \left(\frac{\epsilon(1+d_0)}{3} \right)^{(J-1)N} \left(\frac{\epsilon(2+d_0)}{3} \right)^N \|e_0\|_X \\ &\leq \left(\frac{\epsilon(1+d_0)}{3} \right)^{J-1} \frac{\Delta k}{\sqrt{\alpha}} \left\{ \left(d_0 \frac{\sqrt{\epsilon}\sigma}{\sqrt{3-\epsilon}} + \frac{d_2}{2} \right) \frac{1}{1 - \left(\frac{\epsilon(1+d_0)}{3} \right)^{J-1} \frac{\epsilon(2+d_0)}{3}} \right. \\ &\quad \left. + \left(\frac{\epsilon(1+d_0)}{3} \right)^{(J-1)(N-1)} \frac{N \left(\frac{\epsilon(2+d_0)}{3} \right)^N}{k_h - k_l} d_0 c_0 \left(\frac{\sqrt{\epsilon}\sigma}{\sqrt{3-\epsilon}} \right)^3 \right\}. \end{aligned} \quad (38)$$

From (22) we can see that c_0 is bounded from above by

$$c_0 \leq \frac{4\epsilon}{27d_1d_3}. \quad (39)$$

Moreover, for a fixed frequency interval $[k_l, k_h]$, $N\epsilon^N$ is bounded in terms of N . Therefore, there exists a constant $C^* > 0$ independent of N and α such that

$$\begin{aligned} &\left(d_0 \frac{\sqrt{\epsilon}\sigma}{\sqrt{3-\epsilon}} + \frac{d_2}{2} \right) \frac{1}{1 - \left(\frac{\epsilon(1+d_0)}{3} \right)^{J-1} \frac{\epsilon(2+d_0)}{3}} \\ &+ \left(\frac{\epsilon(1+d_0)}{3} \right)^{(J-1)(N-1)} \frac{N \left(\frac{\epsilon(2+d_0)}{3} \right)^N}{k_h - k_l} d_0 c_0 \left(\frac{\sqrt{\epsilon}\sigma}{\sqrt{3-\epsilon}} \right)^3 \leq C^*. \end{aligned} \quad (40)$$

On the other hand, it follows from (34) that $\sqrt{\frac{\Delta k}{\alpha}} \leq \sqrt{\frac{4\epsilon}{27d_1d_4}}$. Replacing these inequalities into (38) we obtain (23) with $C_1 = C^* \sqrt{\frac{4\epsilon}{27d_1d_4}}$. \square

In the case of noisy data, we have the following result.

Theorem 2.5. *Assume that the radial functions $\tilde{r}(k_n)$ and the subspaces $X_n, n = 0, \dots, N$, are as in Theorem 2.4. Let $r_n, n = 0, \dots, N$, be given by Algorithm 2.1. For fixed positive real numbers $\epsilon, \xi, 0 < \epsilon < 3/(2+d_0), 0 < \xi < 1$, and for the parameters α and c_0 satisfying (20) and (22) respectively, we define the positive parameter $\tilde{\delta}_0$ by*

$$\tilde{\delta}_0 := 2\xi \left[1 - \frac{\epsilon(2+d_0)}{3} \right] d_0 c_0 \alpha^{3/2}. \quad (41)$$

Then there exists an integer N_0 independent of $\tilde{\delta}$ such that if (21) is satisfied, we have $r_n(t) > 0 \forall t \in [0, 2\pi]$ and the following error estimate holds true

$$\|\tilde{r}(k_h) - r_N\|_X \leq C_2 \tilde{\delta}^{2/3} + \left(\frac{\epsilon(1+d_0)}{3} \right)^{J-1} C_1 \sqrt{\Delta k}, \quad \forall N \geq N_0 \quad (42)$$

for every $\tilde{\delta} \leq \tilde{\delta}_0$, where C_1 is as in Theorem 2.4 and C_2 is a constant independent of $\tilde{\delta}, \alpha$ and N .

Proof. Using (13) we can rewrite the error as

$$e_{n+1}^{j+1} = \tilde{r}(k_{n+1}) - r_{n+1}^j + P_{n+1} R_{n+1}^j \tilde{F}(r_{n+1}^j, k_{n+1}) + P_{n+1} R_{n+1}^j f^{\tilde{\delta}}(\tilde{r}(k_{n+1}), k_{n+1}) \quad (43)$$

for $j = 0, \dots, J-1$. It follows from Lemma 2.3 that

$$\|P_{n+1} R_{n+1}^j f^{\tilde{\delta}}(\tilde{r}(k_{n+1}), k_{n+1})\|_X \leq \frac{\tilde{\delta}}{2\sqrt{\alpha}}. \quad (44)$$

Using the estimates (31) and (37) for the noiseless case, from (43)–(44) we have

$$\begin{aligned} \|e_{n+1}^1\|_X &\leq \Delta k \left(d_0 + \frac{d_2}{2\sqrt{\alpha}} \right) + \frac{\tilde{\delta}}{2\sqrt{\alpha}} + \frac{\alpha}{\alpha + \sigma^2} \|e_n\|_X \\ &\quad + \frac{9d_1d_4}{4\alpha} \Delta k \|e_n\|_X + \left(\frac{9d_1d_3}{4\alpha} + \frac{d_3}{4\sqrt{\alpha}} \right) \|e_n\|_X^2. \end{aligned} \quad (45)$$

And for $j = 0, \dots, J-1$, we obtain

$$\|e_{n+1}^{j+1}\|_X \leq \frac{\tilde{\delta}}{2\sqrt{\alpha}} + \frac{\alpha}{\alpha + \sigma^2} \|e_{n+1}^j\|_X + \left(\frac{9d_1d_3}{4\alpha} + \frac{d_3}{4\sqrt{\alpha}} \right) \|e_{n+1}^j\|_X^2. \quad (46)$$

For $\tilde{\delta} \leq \tilde{\delta}_0$, we have from (20) and (41) that

$$\left(\frac{\tilde{\delta}}{2\xi \left[1 - \frac{\epsilon(2+d_0)}{3} \right] d_0 c_0} \right)^{2/3} \leq \alpha \leq \frac{\epsilon}{3-\epsilon} \sigma^2.$$

Or, equivalently, α satisfies (32) and the following inequality

$$\frac{\tilde{\delta}}{2\sqrt{\alpha}} \leq \xi \left[1 - \frac{\epsilon(2+d_0)}{3} \right] d_0 c_0 \alpha. \quad (47)$$

On the other hand, there exists N_0 such that condition (34) is satisfied for all $N > N_0$ and

$$\Delta k \left(d_0 + \frac{d_2}{2\sqrt{\alpha}} \right) \leq (1-\xi) \left[1 - \frac{\epsilon(2+d_0)}{3} \right] d_0 c_0 \alpha, \quad (48)$$

Now using the same arguments as in the proof of Theorem 2.4, we can show that $\|e_n^j\|_X \leq d_0 c_0 \alpha$ for all $j = 0, \dots, J; n = 1, \dots, N$, if (21) is satisfied. This implies the positivity of r_n as in Theorem 2.4. Moreover,

$$\begin{aligned} \|e_{n+1}^1\|_X &\leq \Delta k \left(d_0 + \frac{d_2}{2\sqrt{\alpha}} \right) + \frac{\tilde{\delta}}{2\sqrt{\alpha}} + \frac{\epsilon(2+d_0)}{3} \|e_n\|_X, \\ \|e_{n+1}^{j+1}\|_X &\leq \frac{\tilde{\delta}}{2\sqrt{\alpha}} + \frac{\epsilon(1+d_0)}{3} \|e_{n+1}^j\|_X, j = 1, \dots, J-1. \end{aligned} \quad (49)$$

Consequently, for $n = 0, \dots, N-1$, we have

$$\|e_{n+1}\|_X \leq \frac{\tilde{\delta}}{2\sqrt{\alpha}} \frac{1}{1 - \frac{\epsilon(1+d_0)}{3}} + \left(\frac{\epsilon(1+d_0)}{3} \right)^{J-1} \left[\Delta k \left(d_0 + \frac{d_2}{2\sqrt{\alpha}} \right) + \frac{\epsilon(2+d_0)}{3} \|e_n\|_X \right]. \quad (50)$$

Hence,

$$\begin{aligned} \|e_N\|_X &\leq \frac{\tilde{\delta}}{2\sqrt{\alpha} \left[1 - \frac{\epsilon(1+d_0)}{3} \right] \left[1 - \left(\frac{\epsilon(1+d_0)}{3} \right)^{J-1} \frac{\epsilon(2+d_0)}{3} \right]} \\ &\quad + \left(\frac{\epsilon(1+d_0)}{3} \right)^{J-1} C_1 \sqrt{\Delta k}. \end{aligned} \quad (51)$$

Here the constant C is the same as in Theorem 2.4. Finally, taking into account the condition (47) we obtain (42) with the constant C_2 given by

$$C_2 = \frac{(\xi d_0 \frac{4\epsilon}{27d_1d_3})^{1/3}}{\left[2 \left(1 - \frac{\epsilon(1+d_0)}{3} \right) \right]^{2/3} \left[1 - \left(\frac{\epsilon(1+d_0)}{3} \right)^{J-1} \frac{\epsilon(2+d_0)}{3} \right]}.$$

The proof is complete. \square

Remark 2.2. To obtain the Hölder type error estimate of the form $\|e_N\|_X = O(\tilde{\delta}^{2/3})$, we require that $\left(\frac{\epsilon(1+d_0)}{3} \right)^{J-1} \sqrt{\Delta k} = O(\tilde{\delta}^{2/3})$. That means, if Δk is small, we do not need to use many Newton iterations and vice-versa. In other words, there is a trade-off between the frequency step Δk and the number of Newton iterations for a given accuracy.

2.3 Discussion on the link between the true shape and the observable shapes

Theorems 2.4 and 2.5 show the accuracy of the reconstruction of the observable shapes. The final accuracy of the algorithm with respect to the true shape depends on the stability of the reconstruction problem under investigation. When the final frequency k_h is very high, a Hölder type stability estimate was proved in [25] for the part of the boundary illuminated by the incident wave. Hence a natural question arises: are the error estimates of Theorems 2.4 and 2.5 uniform with respect to frequency interval when k_h becomes very large. The answer to this question depends on the dependence of the constants C_1 and C on the frequency interval. For simplicity, we assume that the lowest frequency is fixed and the same frequency step is used in all frequency intervals. Below we give a heuristic, non-rigorous explanation about which factors could affect the error estimates when k_h increases.

First of all, we know that the higher the frequency, the better the stability of the reconstruction problem. Therefore the observable shapes should become closer and closer. As a result, the constant d_0 in Assumption 2 should not increase when k_h is increased. Second, we can see from (15) that d_1 , d_2 and d_3 are non-decreasing. Moreover, since c_0 can be bounded from above by a constant which is not increased when k_h increases, see (39). Therefore, the constant C_2 is non-increasing.

Concerning the constant C_1 , from (40) it follows that the second term is non-increasing. Indeed, for a given frequency step Δk , we have

$$\frac{N \left(\frac{\epsilon(2+d_0)}{3} \right)^N}{k_h - k_l} = \frac{\left(\frac{\epsilon(2+d_0)}{3} \right)^N}{\Delta k}.$$

That means, it is non-increasing when k_h increases if the frequency step is kept fixed. The other factors of the second term of (40) are clearly non-increasing. Hence, the only factor which could cause the constant C_1 to increase is d_2 in the first term of (40).

The question on how this factor d_2 depends on the frequency is still open to us. Note however that, based on integral equation methods, precisely the explicit dependence of the norms of the corresponding boundary integral operators in terms of the frequencies, see [6, 21] for instance, we infer that d_2 increases as k_h increases, but at a moderate rate, i.e. polynomially. Then we can eliminate its effect on the constant C_1 by increasing the number of Newton steps at each frequency. We will investigate this question in a future work.

3 Multi-level Newton method

In this section, we discuss how to obtain the comparable error estimates as in the previous section but with a less restrictive condition than (21) concerning the reconstruction at the lowest frequency. For this purpose, we use a multi-level Newton method which is described hereafter.

We recall that the error estimate (42) was obtained under the conditions (32), (34), (47) and (48). In this section, we choose $\xi = 1/2$ for simplicity. To make the analysis easier to follow, we rewrite the above conditions here

$$\alpha \leq \frac{\epsilon\sigma^2}{3-\epsilon}, \quad (52)$$

$$\frac{9d_1d_4}{4\alpha}\Delta k \leq \frac{\epsilon}{3}, \quad (53)$$

$$\Delta k \left(d_0 + \frac{d_2}{2\sqrt{\alpha}} \right) \leq \frac{1}{2} \left[1 - \frac{\epsilon(2+d_0)}{3} \right] d_0c_0\alpha, \quad (54)$$

$$\frac{\tilde{\delta}}{2\sqrt{\alpha}} \leq \frac{1}{2} \left[1 - \frac{\epsilon(2+d_0)}{3} \right] d_0c_0\alpha, \quad (55)$$

with the constant c_0 being given by (22) which depends on α . Therefore, in the following, we denote by $c_0(\alpha)$ to indicate this dependence. We reserve the notations c_0 and α for the constants in the previous section, i.e. these constants associate with the full frequency set. So Theorem 2.5 says that if the conditions (52)–(55) are satisfied, and if the solution r_0 at the lowest wavenumber k_0 satisfies (21), i.e.

$$\|\tilde{r}(k_l) - r_0\|_X \leq d_0c_0\alpha < \tilde{c}, \quad (56)$$

then the final error estimate (42) holds true.

We remark that the regularization parameter α depends on the smallest singular value σ of the domain derivative $\tilde{A}_n, n = 0, 1, \dots, N$. Clearly, the more frequencies used, the smaller this singular value σ is. Therefore, by subdividing the original interval of frequencies into sub-intervals and choosing this regularization parameter depending on the smallest singular value in different frequency sub-intervals, we may not need to choose a small regularization parameter (in other words, with a less restrictive condition on the initial guess) at the first sub-interval but still obtain a comparable error estimate as (42).

To make the following analysis consistent with the previous section, we still consider the set of frequencies $k_0 = k_l, \dots, k_N = k_h$ with step size Δk as in section 2. Suppose that the original frequency interval $\{k_0, \dots, k_N\}$ is divided into M sub-intervals from low to high frequencies. These sub-intervals do not need to have the same number of frequencies. We denote by $\tilde{\sigma}_m$ the smallest singular value in the m -th sub-interval. That is,

$$\tilde{\sigma}_m = \min\{\sigma_n, k_n \text{ belongs to the } m\text{-th sub-interval}\}.$$

Here σ_n the smallest singular value of $\tilde{A}_n|_{X_{n+1}}$ as in section 2. Moreover, we choose the sequence of parameters $\hat{\sigma}_m, m = 1, \dots, M$, as follows:

$$\hat{\sigma}_1 = \tilde{\sigma}_1, \quad \hat{\sigma}_{m+1} = \min\{\hat{\sigma}_m, \tilde{\sigma}_{m+1}\}, m = 1, \dots, M-1.$$

by this choice of the parameters $\hat{\sigma}_m$, it is clear that

$$\hat{\sigma}_1 \geq \hat{\sigma}_2 \geq \dots \geq \hat{\sigma}_M \geq \sigma. \quad (57)$$

Associated with these sub-intervals, we choose the set of regularization parameters α_m , $m = 1, \dots, M$ such that (52) is satisfied in each sub-intervals, where σ is replaced by the corresponding parameter $\hat{\sigma}_m$. That is,

$$\alpha_m \leq \frac{\epsilon \hat{\sigma}_m^2}{3 - \epsilon}, m = 1, \dots, M. \quad (58)$$

Moreover, α_m are also chosen such that

$$\alpha_1 \geq \alpha_2 \geq \dots \geq \alpha_M \geq \alpha. \quad (59)$$

The multi-level Newton algorithm can be summarized as follows.

Algorithm 3.1.

- Given measured data $u_m^{\infty, \delta}(\cdot, k)$ for $k = k_0, \dots, k_N$, and the partition of this frequency interval into M sub-intervals.
- Step 1: find an approximation $r_0 \in X_0$ at frequency k_0 .
- Step 2: For $m = 1, \dots, M$
 - Choose α_m satisfying (58) and (59).
 - Use Algorithm 2.1 to find an approximation in the m -th frequency sub-interval.

Let us show a similar convergence result as in Theorem 2.5 for this algorithm. From (22) and (59) it can be proved using elementary analysis that

$$c_0(\alpha_1)\alpha_1 \geq c_0(\alpha_2)\alpha_2 \geq \dots \geq c_0(\alpha_M)\alpha_M \geq c_0\alpha. \quad (60)$$

We recall that c_0 and α are associated with the whole frequency interval $\{k_0, \dots, k_N\}$. It also follows from (59) and (60) that the inequalities (53)–(55) still hold for the same frequency step Δk and noise level as in Theorems 2.4 and 2.5 when α is replaced by α_m and c_0 by $c_0(\alpha_m)$. That means, all the conditions of these theorems are satisfied for each sub-interval.

Now we replace the condition (21) in Theorems 2.4 and 2.5 by the following one for the first sub-interval:

$$\|\tilde{r}(k_l) - r_0\|_X \leq d_0 c_0(\alpha_1) \alpha_1 < \tilde{c}. \quad (61)$$

Hence, from Theorem 2.5 (see (51)) we obtain the following error estimate in the first

sub-interval

$$\begin{aligned}
\|\tilde{r}(k_{N_1}) - r_{N_1}\|_X &\leq \frac{\tilde{\delta}}{2\sqrt{\alpha_1} \left[1 - \frac{\epsilon(1+d_0)}{3}\right] \left[1 - \left(\frac{\epsilon(1+d_0)}{3}\right)^{J-1} \frac{\epsilon(2+d_0)}{3}\right]} \\
&+ \tilde{C}_1 \left(\frac{\epsilon(1+d_0)}{3}\right)^{J-1} \sqrt{\Delta k}. \\
&\leq \frac{\tilde{\delta}}{2\sqrt{\alpha} \left[1 - \frac{\epsilon(1+d_0)}{3}\right] \left[1 - \left(\frac{\epsilon(1+d_0)}{3}\right)^{J-1} \frac{\epsilon(2+d_0)}{3}\right]} \\
&+ \tilde{C}_1 \left(\frac{\epsilon(1+d_0)}{3}\right)^{J-1} \sqrt{\Delta k}. \tag{62}
\end{aligned}$$

for a constant \tilde{C}_1 . This constant can be chosen fixed for all frequency sub-intervals and independent of $\tilde{\delta}$. Here k_{N_1} is the maximum frequency of the first sub-interval. It follows from (54) and (62) that

$$\|\tilde{r}(k_{N_1}) - r_{N_1}\|_X \leq \frac{d_0 c_0 \alpha}{2 \left[1 - \left(\frac{\epsilon(1+d_0)}{3}\right)^{J-1} \frac{\epsilon(2+d_0)}{3}\right]} + \tilde{C}_1 \left(\frac{\epsilon(1+d_0)}{3}\right)^{J-1} \sqrt{\Delta k}. \tag{63}$$

In the second sub-interval, we use the final approximation r_{N_1} of the first sub-interval as the initial guess, i.e., it plays the same role as r_0 in section 2. For the given frequency step Δk , we can choose the number of Newton iterations J large enough so that the following inequality holds true

$$\|\tilde{r}(k_{N_1}) - r_{N_1}\|_X \leq d_0 c_0 \alpha_2. \tag{64}$$

This process can be continued until the last sub-interval. In the last sub-interval, we obtain a similar error estimate as (42). We summarize the above analysis in the following theorem.

Theorem 3.2. *Suppose that the frequency set $\{k_0, \dots, k_N\}$ is subdivided into M sub-intervals. Denote by N_m the number of frequencies in the m -th sub-interval. Moreover, let ϵ be a positive real number satisfying $0 < \epsilon < 3/(2+d_0)$, and α_m , $m = 1, \dots, M$, be the regularization parameters satisfying (58) and (59). We also suppose that the frequency step is small enough so that the conditions (53) and (54) are fulfilled for $\alpha = \min\{\alpha_m, m = 1, \dots, M\}$ and $c_0 = c_0(\alpha)$ given by (22). Then there exists an integer J large enough such that if the reconstruction at the lowest frequency satisfies (61), we have $r_n(t) > 0 \forall t \in [0, 2\pi]$ and the following error estimate holds true*

$$\|\tilde{r}(k_h) - r_N\|_X \leq C_2 \tilde{\delta}^{2/3} + \left(\frac{\epsilon(1+d_0)}{3}\right)^{J-1} \tilde{C}_1 \sqrt{\Delta k}, \tag{65}$$

for every $\tilde{\delta} \leq \tilde{\delta}_0$, where C_2 is as in Theorem 2.5 and \tilde{C}_1 is a constant independent of $\tilde{\delta}$, α_m and N . Here $\tilde{\delta}_0$ is defined as in (41).

Remark 3.1. *Theorem 3.2 indicates that we still obtain the same error estimate as in Theorem 2.5 with C_1 being replaced by \tilde{C}_1 . That means, by using the multi-level algorithm, we can obtain basically the same error estimate as in Theorem 2.5 with the first guess r_0 satisfying the condition (61) which is, in general, weaker than (21) due to (60). This issue is related to estimating the lower bounds of the singular values σ_1 . Actually, at each level m , $m = 1, \dots, M$, we take the regularization parameter α satisfying similar estimate, i.e (58). In a forthcoming work, we will investigate the lower bound of σ_m in terms of the frequency κ and the dimension of the corresponding space X_{n+1} . With such estimates at hand, the regularization parameter α_m can be chosen compared to the known quantities k and n . Let us finally make some comments on the condition (55) on the noise level. As the frequency becomes high, α becomes small and so for the noise level. However this is quite natural since at high frequencies we expect to reconstruct small details and this makes sense only if the measurements at hand are not so noisy.*

4 Numerical results

In this section, we show some numerical results to demonstrate the performance of the proposed algorithms. We also compare reconstruction results using these algorithms with the recursive linearization algorithm.

In these tests, we considered flower-shaped obstacles defined by the equation

$$\{x(t) = c_1(1 + c_2 \cos c_3 t)(\cos t, \sin t), t \in [0, 2\pi)\}$$

with positive constants c_1 , c_2 and c_3 . The first parameter determines the area of the obstacle, the second one relates to the curvature and the last one determines the number of petals of the "flower". Two obstacles were considered which correspond to two sets of parameters: $c_1 = 2$, $c_2 = 0.3$ and $c_3 = 4$ (obstacle 1), and $c_1 = 2$, $c_2 = 0.2$ and $c_3 = 9$ (obstacle 2).

The measured far field patterns $u_m^\infty(\cdot, k_j, r)$, $j = 0, \dots, N$, used in these tests were simulated as the solution of the forward problem (1)–(3) which was solved by the integral equation method [10]. We used 16 observation directions uniformly distributed on the unit circle. The same method was also used to calculate the domain derivative of the far field operator. Additive random noise of 5% was added to the computed far field patterns.

Our numerical tests in [25] have indicated that although the regularization parameter α must satisfies conditions (32) and (47) in the theoretical analysis, numerical performance seemed to be more optimistic. In our tests, this parameter could be chosen in a wide range, say, from 10^{-6} to 10^{-1} which still provided good reconstruction results. Therefore, in the following examples, the regularization parameter α was chosen to be 10^{-2} . We fixed the direction of incidence to be $\theta = (-\frac{1}{2}, \frac{\sqrt{3}}{2})$. The wavenumbers were chosen between $k_l = 0.5$ and $k_h = 8$.

The approximation r_0 at the lowest frequency was computed as follows: we first approximated the obstacle by a circle. In this case, the center and radius of the approximating circle were found by minimizing the corresponding least-squares objective functional.

Then, three Fourier coefficients were chosen to represent r_0 . These parameters were then found by solving again the least-squares minimization problem using the Matlab optimization routine *fmincon*. Our results showed that these optimization problems were stable, therefore we did not need a good initial guess. However, we obtained only an approximation of the low frequency information of the obstacle in this step.

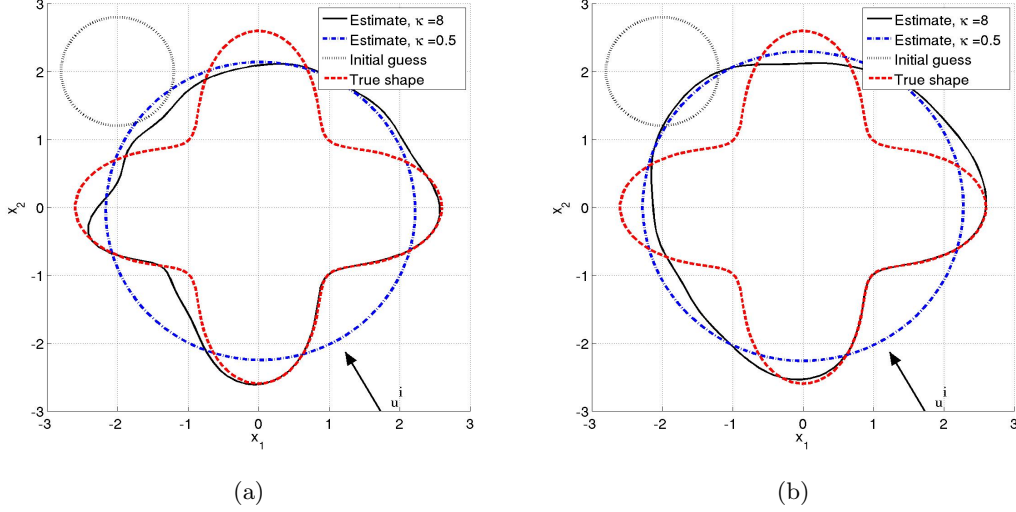


Figure 1: Reconstruction of obstacle 1 using 12 wavenumbers: (a) 4 Newton iterations; (b) 1 Newton iteration.

Figure 1 shows the reconstruction of obstacle 1 using 12 wavenumbers. In Figure 1(a), 4 Newton iterations at each frequency were used while only 1 Newton iteration at each frequency was used in Figure 1(b). We can see that the first one is more accurate than the second one. We remark that, as pointed out in [25], the reconstruction is good in the part of the obstacle illuminated by the incident plane wave but the details of the shadow part is not well reconstructed.

In Figure 2 we depict the reconstruction of obstacle 2. For this obstacle, 20 wavenumbers were used in order to reconstruct its small detailed features. We also can see that using 4 Newton iterations improved the accuracy compared to using only 1 iteration. We would like to emphasize that this improvement is more clear for a smaller number of frequencies or a larger number of Newton iterations, see Figure 3 for the results of obstacle 2 using 16 wavenumbers.

To see the performance of the multi-level method of Section 3, we show in Figure 4 the reconstruction of the two obstacles. The reconstruction r_0 at the lowest frequency was obtained by just one iteration of the nonlinear least-squares optimization problem. By doing so, we expected that this should not be as good as in the previous tests. The regularization parameter α at the first frequency step was chosen to be 0.04 which is 4 times larger than that at the other frequencies. Moreover, 5 iterations were used at the first step

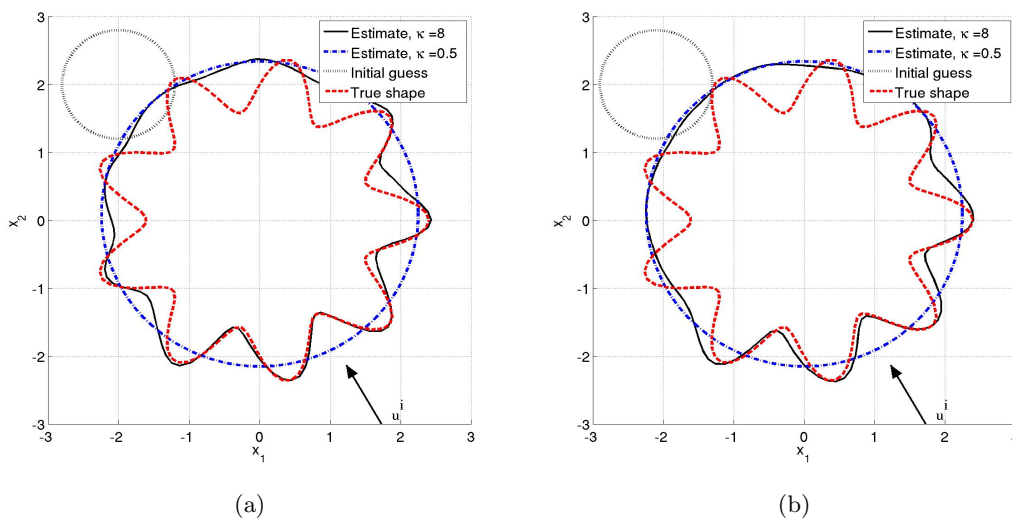


Figure 2: Reconstruction of obstacle 2 using 20 wavenumbers: (a) 4 Newton iterations; (b) 1 Newton iteration.

and 4 iterations were used at the other frequencies. As can be seen, the reconstructions are comparable to Figure 1(a) and Figure 2(a) which confirm our theoretical analysis.

Acknowledgments

M. Sini was supported by the Johann Radon Institute for Computational and Applied Mathematics (RICAM), Austrian Academy of Sciences and by the Austrian Science Fund (FWF) under the project No. P22341-N18. N. T. Thành was supported by US Army Research Laboratory and US Army Research Office grants W911NF-11-1-0399.

References

- [1] G. Alessandrini and L. Rondi. Determining a sound-soft polyhedral scatterer by a single far-field measurement. *Proc. Amer. Math. Soc.*, 133(6):1685–1691, 2005.
- [2] H. Ammari, J. Garnier, H. Kang, M. Lim, and K. Sølna. Multistatic imaging of extended targets. *SIAM J. Imaging Sci.*, 5(2):564–600, 2012.
- [3] G. Bao and F. Triki. Error estimates for the recursive linearization of inverse medium problems. *Journal of Computational Mathematics*, 28(6):725–744, 2010.
- [4] K. Belkebir, S. Bonnard, F. P. an P. Sabouroux, and M. Saillard. Validation of 2D inverse scattering algorithms from multi-frequency experimental data. *Journal of Electromagnetic Waves and Applications*, 14:1637–1667, 2000.

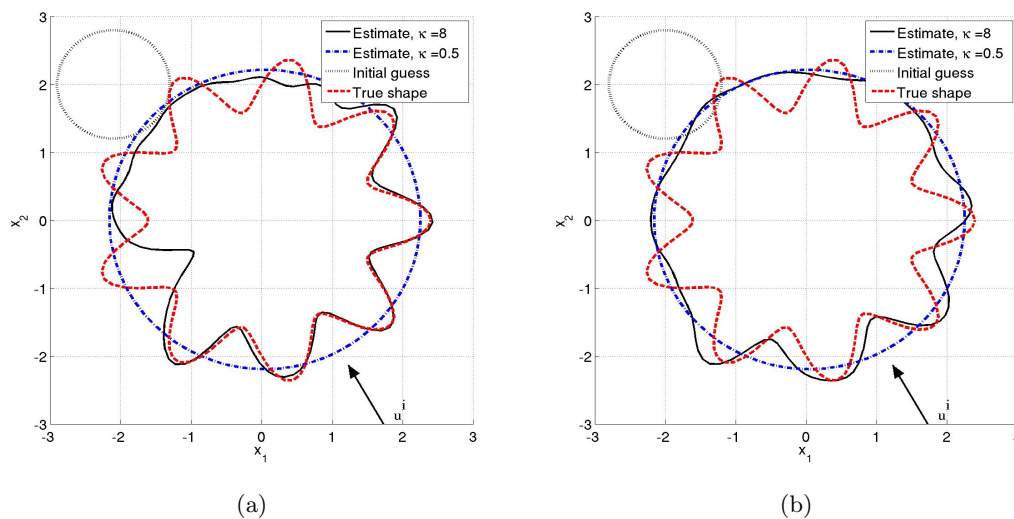


Figure 3: Reconstruction of obstacle 2 using 16 wavenumbers: (a) 10 Newton iterations; (b) 1 Newton iteration.

- [5] O. Bucci and T. Isernia. Electromagnetic inverse scattering: Retrievable information and measurement strategies. *Radio Sci.*, 32(6):2132–2138, 1997.
- [6] S. N Chandler-Wilde and P. Monk. Wave-number-explicit bounds in time-harmonic scattering. *SIAM J. Math. Anal.* 39 (2008), no. 5, 1428–1455.
- [7] Y. Chen. Inverse scattering via Heisenberg’s uncertainty principle. *Inverse Problems*, 13(2):253–282, 1997.
- [8] J. Cheng and M. Yamamoto. Global uniqueness in the inverse acoustic scattering problem within polygonal obstacles. *Chinese Ann. Math. Ser. B*, 25(1):1–6, 2004.
- [9] W. Chew and J. Lin. A frequency-hopping approach for microwave imaging of large inhomogeneous bodies. *IEEE Microwave and Guided Wave Letters*, 5:439–441, 1995.
- [10] D. Colton and R. Kress. *Inverse acoustic and electromagnetic scattering theory*. Springer-Verlag, Berlin, second edition, 1998.
- [11] D. Colton and B. D. Sleeman. Uniqueness theorems for the inverse problem of acoustic scattering. *IMA J. Appl. Math.*, 31(3):253–259, 1983.
- [12] M. V. de Hoop, L. Qiu, and O. Scherzer. A convergence analysis of a multi-level projected steepest descent iteration for nonlinear inverse problems in banach spaces subject to stability constraints. Preprint, arXiv:1206.3706 [math.NA].
- [13] G. B. Folland. *Fourier Analysis and Its Applications*. Wadsworth & Brooks/Cole Advanced Books & Software, Pacific Grove, CA, 1992.

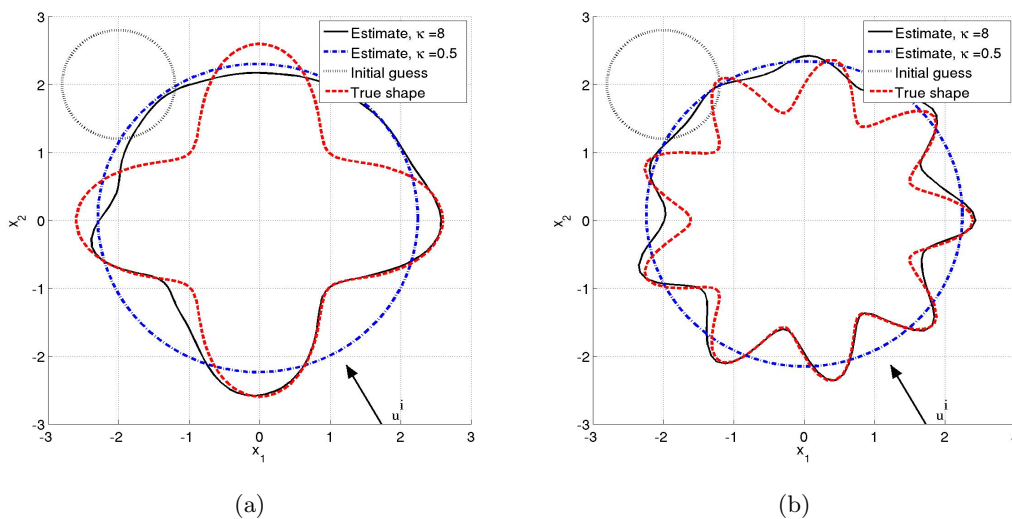


Figure 4: Reconstruction using the multi-level Newton method: (a) obstacle 1 with 12 wavenumbers; (b) obstacle 2 with 20 wavenumbers.

- [14] D. Gintides. Local uniqueness for the inverse scattering problem in acoustics via the Faber-Krahn inequality. *Inverse Problems*, 21(4):1195–1205, 2005.
- [15] R. Griesmaier. Multi-frequency orthogonality sampling for inverse obstacle scattering problems. *Inverse Problems*, 27(8):085005, 23, 2011.
- [16] B. B. Guzina, F. Cakoni, and C. Bellis. On the multi-frequency obstacle reconstruction via the linear sampling method. *Inverse Problems*, 26(12):125005, 29, 2010.
- [17] N. Honda, G. Nakamura, and M. Sini. Analytic extension and reconstruction of obstacles from few measurements for elliptic second order operators. *Math. Ann.*, 355 (2013), no. 2, 401-427.
- [18] V. Isakov. *Inverse Problems for Partial Differential Equations*. Springer, New York, second edition, 2006.
- [19] A. Kirsch. The domain derivative and two applications in inverse scattering theory. *Inverse Problems*, 9(1):81–96, 1993.
- [20] W. McLean. *Strongly Elliptic Systems and Boundary Integral Equations*. Cambridge University Press, Cambridge, 2000.
- [21] J. M. Melenk. Mapping properties of combined field Helmholtz boundary integral operators. *SIAM J. Math. Anal.* 44 (2012), no. 4, 2599-2636.
- [22] R. Potthast. A study on orthogonality sampling. *Inverse Problems*, 26:074015(17pp), 2010.

- [23] A. G. Ramm. *Multidimensional Inverse Scattering Problems*. Longman Scientific & Technical, Harlow, 1992.
- [24] E. Sincich and M. Sini. Local stability for soft obstacles by a single measurement. *Inverse Probl. Imaging*, 2(2):301–315, 2008.
- [25] M. Sini and N. T. Thành. Inverse acoustic obstacle scattering problems using multi-frequency measurements. *Inverse Problems and Imaging*, 6(4):749–773, 2012.
- [26] P. Stefanov and G. Uhlmann. Local uniqueness for the fixed energy fixed angle inverse problem in obstacle scattering. *Proc. Amer. Math. Soc.*, 132(5):1351–1354 (electronic), 2004.
- [27] A. Tjhuis, K. Belkebir, A. Litman, and B. de Hon. Multi-frequency distorted-wave Born approach to 2D inverse profiling. *Inverse Problems*, 17:1635–1644, 2001.
- [28] A. Tjhuis, K. Belkebir, A. Litman, and B. de Hon. Theoretical and computational aspects of 2-D inverse profiling. *IEEE Transactions on Geoscience and Remote Sensing*, 39(6):1316–1330, 2001.